Available online at www.sciencedirect.com
ScienceDirect
Aerosol Science 38 (2007) 532–549
Journal of Aerosol Science
www.elsevier.com/locate/jaerosci

A microsphere-surface impact model for implementation in computational fluid dynamics

O.V. Kim, P.F. Dunn*

Particle Dynamics Laboratory, Department of Aerospace and Mechanical Engineering, University of Notre Dame, 107 Hessert Laboratory, Notre Dame, IN 46556, USA

Received 7 December 2006; received in revised form 26 February 2007; accepted 7 March 2007

Abstract

Two microsphere-surface impact models have been developed for implementation with computational fluid dynamic software. The models consider either normal or oblique incidence of a microsphere with the surface. The first model includes the effects of microsphere-surface roughness, and Hertzian and adhesion damping during surface contact. The second model considers the impact of elastic–plastic sphere and a surface, with and without interface adhesion. Analytical solutions for the coefficients of restitution are presented in terms of the impact velocity and material properties. These algebraic models were validated by comparison with the experimental results of several investigators. A user-defined function representing the model was developed to interface with the commercial software package FLUENT®. The combined modelling package's predictions were compared with high-speed digital images of microparticle contact with the surface located on the floor of a wind tunnel.

Keywords: Microparticle; Surface; Impact; Computational fluid dynamics

1. Introduction

Particle impact with a surface can occur over a wide range of incident velocities. In practice, both low-speed and very high-speed impacts are of particular interest. Low-speed impacts (less than approximately 10 m/s) occur in situations such as filtering, surface cleaning, and in the ducts of heating, ventilation, and air-conditioning (HVAC) systems. Very high-speed impacts (greater than approximately several hundred m/s) are of great importance in aerospace applications.

The physical nature of contact between a particle and a surface varies with impact speed and the size of the particle. The low-speed impact of a particle whose diameter is greater than approximately 100 μm can be considered to be primarily elastic. For smaller particles (microparticles), adhesion effects also must be considered. Further, high rates of strain occur because of the microparticle's short surface-contact time (∼ μs). Mechanical properties of the microparticle, such as its yield strength, can change by several orders of magnitude (Sagomonyan, 1988; Tabor, 1948). For higher impact speeds (up to ∼100 m/s), the inertial resistance of the material (proportional to square of the velocity) must be considered. Deformation is highly nonuniform. Temperature effects on material properties as well as some plastic deformation can occur. For very high-speed impacts, the particle's incident kinetic energy is high enough to melt both

* Corresponding author.
E-mail address: patrick.f.dunn.1@nd.edu (P.F. Dunn).

0021-8502/$ - see front matter © 2007 Elsevier Ltd. All rights reserved.
doi:10.1016/j.jaerosci.2007.03.006

the particle and some of the impact surface upon impact (Klinkov, Kosarev, & Rein, 2005). This can damage the surface of a flight vehicle. Hydrodynamic theory can be used to describe movement of the liquified impact surface and particle.

This paper presents two models of the impact event of a microsphere with a surface. The first model, termed the EA model, considers an elastic impact with adhesion. The particle's kinetic energy is related to static elastic and adhesion forces and their dynamic dissipative forces. In the second model, termed the EAP model, plastic effects that occur with ductile materials are considered in addition to elastic and adhesion effects. Both models are based upon the governing equations of motion of a microsphere while in contact with flat surface.

A number of microsphere/surface impact models have been presented over the past 30 years. Several models have been developed to predict microsphere behavior *after* impact with a surface (Andres, 1995; Brach & Dunn, 1995; Brach, Dunn, & Li, 2000; Dahneke, 1975; Thornton & Ning, 1998; Tsai, Pui, & Liu, 1991; Wall, John, Wang, & Goren, 1990; Xu & Willeke, 1993). All of these models require some empirically based information (such as the amount of secondary elastic deformation or the effective inertial mass of the substrate) that must be known *a priori* to compare the model directly with an actual impact situation. This information is in addition to material property values and incident conditions. Further, the values of the material properties used in the models are based upon bulk (macro-scale) materials. This introduces additional uncertainty into modelling this micro-scale problem. The challenge still remains to reliably predict new situations in which no empirical information is known *a priori*.

In the present paper, the model originally proposed by Brach and Dunn (1995) and extended to more complicated situations by Cheng, Brach, and Dunn (2002a) is presented in both dimensional and nondimensional forms. Then, the model's nonlinear differential equations that describe the motion of the microsphere on the surface during contact are approximated by algebraic expressions. A second model is given that is based upon Kadomtsev's elastic–plastic model (Alexandrov, Kadomtsev, & Tsaryuk, 1984). This model is extended to include adhesion effects. The resulting equations of both models can be solved to yield an input/ouput model that can be incorporated readily into a commercial computational fluid dynamics (CFD) software package.

2. The EA model

Brach and Dunn (1995) proposed an impact model in which elastic and adhesion forces are considered. Energy is dissipated through material deformation and adhesion damping (Hunter, 1957). These energy losses are assumed to be independent. The effect of gravity is neglected.

Variables for this model are shown pictorially in Fig. 1. The particle radius is r, the incident velocity, $\mathbf{v}$, and the rebound velocity, $\mathbf{V}$. The coordinate system is Cartesian in the impact plane with axes t (tangential) directed along the surface and n (normal) perpendicular to the surface.

Particle motion in the normal, tangential, and rotational directions, respectively, are

$$m\ddot{n} = F_n = F_{\mathrm{H}} + F_{\mathrm{HD}} + F_{\mathrm{A}} + F_{\mathrm{AD}}, \tag{1}$$

$$m\ddot{t} = F_t, \tag{2}$$

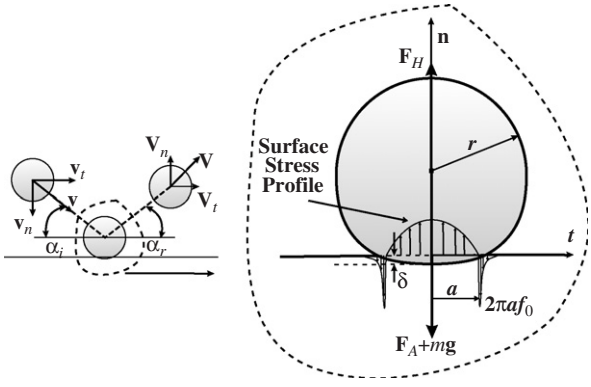

Fig. 1. Schematic of microsphere impact with a planar surface.

and

$$I\ddot{\theta} = rF_t. \tag{3}$$

In these equations, F_{HD} represents Hertzian (material deformation) damping, which equals $C_H F_H$, F_A adhesion damping, which equals $C_A F_A$, and τ time. For the normal direction, where $x = -n$, Eq. (1) can be written as

$$m\ddot{x} = -\sqrt{r}Kx^{3/2} - \sqrt{r}Kx^{3/2}C_H\dot{x} + 2\pi a f_0 - 2\pi a f_0 C_A\dot{x}. \tag{4}$$

The first term on the right-hand side is the classical Hertzian restoring force and is equal to $F_H = \sqrt{r}K(x)^{3/2}$ for $x \geqslant 0$, where n, the relative displacement of the particle's center of mass, is in the negative x direction. F_H and F_A represent the Hertzian and adhesion forces. The variables K, k_i, and r are expressed as

$$K = \frac{4}{3\pi(k_1 + k_2)}, \tag{5}$$

$$k_i = \frac{1 - v_i^2}{\pi E_i}, \tag{6}$$

and

$$r = \frac{R_s r_s}{R_s + r_s}. \tag{7}$$

Here K is Hertzian stiffness (N/m^2), E_i Young's modulus (Pa), v_i Poisson's ratio, and R_s and r_s the radii of the non-deformed sphere and of the local curvature of the surface, respectively.

The nondimensional form of Eq. (4) is

$$\ddot{\tilde{x}} = -\tilde{x}^{3/2}(1 + C_1\dot{\tilde{x}}) + \tilde{x}^{1/2}(1 - C_2\dot{\tilde{x}}), \tag{8}$$

where $\tilde{x} = x/L$ and $\tilde{\tau} = \tau/T$. Expressions for the characteristic length, L, and time, T, scales are

$$L = \frac{2\pi f_0}{K} \tag{9}$$

and

$$T = \frac{m^{1/2}}{(2\pi r f_0 K)^{1/4}}. \tag{10}$$

The nondimensional damping coefficients are

$$C_1 = C_H\frac{L}{T} = C_H\frac{(2\pi f_0)^{5/4}r^{1/4}}{K^{3/4}m^{1/2}}, \tag{11}$$

and

$$C_2 = C_A\frac{L}{T} = C_A\frac{(2\pi f_0)^{5/4}r^{1/4}}{K^{3/4}m^{1/2}}. \tag{12}$$

Eq. (8) is nonlinear and can be solved numerically by using, for example, the Runge–Kutta–Gill method (Cheng et al., 2002a; Cheng, Brach, & Dunn, 2002b).

3. Algebraic approximation of the model

A conservation of energy equation can be obtained from Eqs. (1)–(3). Algebraic approximations of the resulting equation's integrals can made to arrive at an explicit expression for the particle's coefficient of restitution. This expression can be utilized readily in a CFD software package.

The acceleration terms, $\ddot{n}$, $\ddot{t}$, and $\ddot{\theta}$, in Eqs. (1)–(3) become $\mathrm{d}(u_n^2/2)/\mathrm{d}n$, $\mathrm{d}(u_t^2/2)/\mathrm{d}t$, and $\mathrm{d}(\omega^2/2)/\mathrm{d}\theta$, respectively. These expressions can be substituted into the three equations, which are summed and integrated to yield

$$\frac{1}{2}m(u_n^2+u_t^2)|_v^V+\frac{1}{2}I\omega^2|_\omega^\Omega=\int_0^{\delta n}F_n dn+\int_0^{\delta t}F_t dt+\int_0^{\delta\theta}rF_t d\theta. \tag{13}$$

Here δn, δt, and $\delta\theta$ are the displacements in $\mathbf{t}$, $\mathbf{n}$ and θ directions, respectively. Equation (13) can be rearranged to express the conservation of energy of the particle as

$$\frac{mv^2}{2}+\frac{I\omega^2}{2}=\frac{mV^2}{2}+\frac{I\Omega^2}{2}+W_\mathrm{A}+W_\mathrm{diss}. \tag{14}$$

The left-hand side of the equation contains the particle's initial kinetic, $mv^2/2$, and rotational, $I\omega^2/2$, energies. These energies are transformed following rebound into the particle's final kinetic energy, $mV^2/2$, final rotational energy, $I\Omega^2/2$, work of adhesion, W_A, and work of the dissipative forces, W_diss, which equals $W_\mathrm{HD}+W_\mathrm{AD}$. The work of the Hertzian force, W_H, is zero when integrated over the contact duration. The two work terms resulting from tangential and rotational motion are negligible when compared to W_A.

3.1. Normal incidence

In the case of normal incidence, a non-rotating particle will remain so after impact because no tangential forces and moments affect the particle's rotation. Noting that $e\equiv|V_n/v_n|$, Eq. (14) can be rearranged to become

$$e^2=1-\frac{W_\mathrm{A}+W_\mathrm{diss}}{mv_n^2/2}. \tag{15}$$

Consider first the work done by the adhesion force. This force can be represented as an idealized line force $F_\mathrm{A}=2\pi a f_0 C_\mathrm{R}$, where a is the radius of the contact area, C_R is a factor that accounts for surface roughness (to be discussed in Section 5), and f_0 is the circumferential tension of the adhesion force per unit length, which is equal to

$$f_0=\left(\frac{9Krw_\mathrm{A}^2}{2\pi}\right)^{1/3}. \tag{16}$$

Here w_A is the combined surface energy between the sphere and surface material (the energy required to separate the materials). This energy can be obtained through Dupre's equation

$$w_\mathrm{A}=\gamma_1+\gamma_2-\gamma_{12}, \tag{17}$$

where γ_1 and γ_2 are surface free energies of bodies 1 and 2, and γ_{12} is the interfacial energy. This energy can be estimated by

$$\gamma_{12}=\gamma_1+\gamma_2-2\Phi_{12}\sqrt{\gamma_1\gamma_2}, \tag{18}$$

where only dispersion forces are responsible for the interaction between the two materials (Israelachvilli, 1992), and the interfacial parameter Φ_{12} is approximately equal to 1. Timoshenko and Goodier (1951) showed that the work of adhesion, W_A, can be expressed by

$$W_\mathrm{A}=-2a_\mathrm{m}^2F_\mathrm{A}/3r, \tag{19}$$

where a_m, the maximum contact radius given by Hertzian theory, is

$$a_\mathrm{m}=[5r^2mv_n^2/(4K)]^{1/5}. \tag{20}$$

Combining Eqs. (19) and (20) and dividing by $mv_n^2/2$ yields

$$\frac{W_\mathrm{A}}{mv_n^2/2}=2C_\mathrm{R}f_0\left(\frac{4}{3\pi}\right)\left(\frac{5}{4K}\right)^{3/5}\left(\frac{r}{m^2}\right)^{1/5}v_n^{-4/5}=\psi_\mathrm{A}. \tag{21}$$

The absolute value of the dissipative adhesion force is assumed to be given as $F_{AD} = F_A C_A v_n$. Hence, the corresponding energy dissipation is $W_{AD} = W_A C_A v_n$. The absolute value of the dissipative Hertzian force is taken as

$$F_{HD} = F_H C_H v_n = \sqrt{r} K \left(\frac{2a_m^2}{3r}\right)^{3/2} (C_H v_n). \tag{22}$$

The work done by the dissipative Hertzian force, W_{HD}, can be found by using the expression for the total relative displacement of contacting surfaces $\delta \simeq W_A / F_A = 2a_m^2/(3r)$. Introducing a new variable e_H gives

$$e_H = \frac{\delta F_{HD}}{m v_n^2/2} = 2\frac{a_m^5}{mr^2} K (2/3)^{5/2} \left(\frac{C_H}{v_n}\right) = \psi_H C_H. \tag{23}$$

Thus, Eq. (14) can be rewritten as

$$e = \sqrt{1 - (e_A + e_H)} = \sqrt{1 - \psi_A(1 + C_A v_n) - \psi_H C_H}, \tag{24}$$

where $e_A = (\delta F_{AD} + W_A)/(mv^2/2)$, and ψ_A and ψ_H are given by Eqs. (21) and (23).

3.2. Oblique incidence

Tangential motion over a contact surface can be either sliding or rolling. In the case of oblique incidence, the motion during the contact depends on the incident angle, α_i. If $\alpha_i \leqslant \alpha_{crit}$, then the particle is sliding at the end of surface contact. If $\alpha_i > \alpha_{crit}$, then the particle is rolling at the end of surface contact.

Velocity changes in the normal direction are related to velocity changes in the tangential direction through the impulse ratio, μ, which is $(V_t - v_t)/(V_n - v_n)$. The critical angle is determined from equating $\mu_{sliding} = f$ and $\mu_{rolling} = (2/7)(1 + e)v_t/v_n$, where f is the dynamic coefficient of friction. The dependence of critical angle on material properties and the incident conditions can be written as

$$\alpha_{crit} = \arctan[2(1 + e)/(7f)] = \arctan[2(1 + \sqrt{1 - \psi_A(1 + C_A v_n) - \psi_H C_H})]/(7f). \tag{25}$$

The tangential equation of motion is

$$m\ddot{t} = F_t, \tag{26}$$

where, when sliding,

$$F_t = -f\sqrt{r} K n^{3/2} \operatorname{sgn}(\dot{t} - r\dot{\theta}) \quad \text{with } \dot{t} - r\dot{\theta} \neq 0, \tag{27}$$

and, when rolling,

$$F_t = 0 \quad \text{with } \dot{t} - r\dot{\theta} = 0. \tag{28}$$

4. EAP model

When ductile materials are involved in an impact, plastic effects can be significant even at rather low velocities (Gorham & Kharaz, 2000). An analytical solution for the coefficient of restitution can be obtained for this situation. To accomplish this, it is necessary to assume that damping forces are negligibly small (C_A and C_H equal zero).

For the case of developed plastic deformations, the distribution of normal stresses in the contact zone will tend to the distribution of stresses given by a rigid-plastic model. The elastic contribution to the local deformation will be determined by this distribution and not by the Hertzian stresses. Alexandrov et al. (1984) and Biryukov and Kadomtsev (2002) proposed an elastic–plastic model that takes these factors into account. Their model was compared with the experimental results of Kangur and Kleis (1988).

The dependence of the local displacement versus the contact force, $\delta(F)$, given by this model can be written as

$$\delta = \begin{cases} bF^{2/3}, & \text{when } \mathrm{d}F/\mathrm{d}t > 0,\ F_{max} < F_1, \\ b_f F^{2/3} + \delta_p(F_{max}), & \text{when } \mathrm{d}F/\mathrm{d}t < 0,\ F_{max} > F_1, \\ (1 + \beta)c_1\sqrt{F} + (1 - \beta)Fd, & \text{when } \mathrm{d}F/\mathrm{d}t > 0,\ F_{max} > F_1, \end{cases} \tag{29}$$

where $b = R^{-1/3}[3/(4E)]^{2/3}$, $E = E_1E_2[E_1(1-\nu_1^2) + E_2(1-\nu_2^2)]^{-1}$, $F_1 = \eta^3(3R/4E)^2$, and $\eta = \pi k\lambda$. Here $\lambda = 5.7$ and k is the smallest of two plastic constants of the particle and of the surface. Also, $b_f = R_f^{-1/3}(3/(4E))^{2/3}$, $R_f = (4/3)EF_{max}^{1/2}\eta^{-3/2}$, $\delta_{max} = (1-\beta)F_{max}(2\eta R_p)^{-1}$, $R_p^{-1} = R^{-1} - R_f^{-1}$, $\beta = 0.33$, $c_1 = 3\eta^{1/2}(8E)^{-1}$, and $d = (2\eta R)^{-1}$. If the maximum force at the approach phase is less than the yield limit, then Eq. (29) gives the Hertz model expression $\delta = bF^{2/3}$. If the maximum force at the approach phase exceeds the yield limit, the third expression for δ is used. This represents the rigid-plastic model when the elastic terms are ignored (when $c_1 = 0$). During the restitution phase, the second expression is used, where the plastic deformation δ_p is taken into account.

The impact process can be divided into approach and restitution phases. During the approach phase, the equation of motion is integrated from an incident velocity to 0 and a maximum contact force is determined. Then, using the value for the maximum force, the equation of motion is integrated from a zero velocity to a final rebound velocity during the restitution phase. Thus, for the approach phase,

$$-\frac{mv^2}{2} = -\int_0^{F_1} F\frac{d\delta^{(1)}}{dF}dF - \int_{F_1}^{F_{max}} F\frac{d\delta^{(2)}}{dF}dF, \tag{30}$$

where $\delta^{(1)} = bF^{2/3}$ and $\delta^{(2)} = (1+\beta)c_1\sqrt{F} + (1-\beta)Fd$. Eq. (30) can be integrated to arrive at an equation that can be used to determine the maximum contact force, where

$$(1+\beta)\frac{1}{3\sqrt{F_1}}F_{max}^{3/2} + (1-\beta)\frac{F_{max}^2}{2F_1} + F_1(\beta/6 - 1/30) - \frac{mv^2}{\delta_1} = 0. \tag{31}$$

Solving Eq. (31) for F_{max} gives

$$F_{max} = \frac{1}{4}A_1^2 + \frac{1}{2}\sqrt{\frac{1}{4}A_1^4 - \frac{4}{3}A_2 + \frac{16\cdot 2^{1/3}}{3}\frac{A_2^2}{A_3} + \frac{A_3}{3\cdot 2^{1/3}}} - \frac{1}{2}\sqrt{\frac{1}{2}A_1^4 - \frac{8}{3}A_2 - \frac{16\cdot 2^{1/3}}{3}\frac{A_2^2}{A_3} - \frac{A_3}{3\cdot 2^{1/3}} + \frac{A_1^6 - 8A_1^2A_2}{4\left(0.25A_1^4 - (4/3)A_2 + \frac{16\cdot 2^{1/3}}{3}\frac{A_2^2}{A_3} + \frac{A_3}{3\cdot 2^{1/3}}\right)^{0.5}}}, \tag{32}$$

where $A_1 = Q_1/Q_2$, $A_2 = Q_3/Q_2$, $A_3 = (27A_1^4A_2^2 - 128A_2^3 + 3\sqrt{3}A_1^2A_2^2\sqrt{27A_1^4 - 256A_2})^{1/3}$, $Q_1 = (1+\beta)\delta_1F_1^{-1/2}/6$, $Q_2 = (1-\beta)\delta_1F_1^{-1}/4$, and $Q_3 = \delta_1F_1(5\beta - 1)/60 - mv^2/2$.

During the restitution phase, integrating the equation of motion from zero velocity to the final rebound velocity in accordance with Eq. (29) gives

$$V = 2\sqrt{1/(5m)}R_f^{-1/6}[3/(4E)]^{1/3}F_{max}^{5/6}. \tag{33}$$

Finally, the elastic–plastic coefficient of restitution is given by

$$e_{pl} = \left|\frac{V}{v}\right| = \frac{2}{v}\sqrt{1/(5m)}R_f^{-1/6}[3/(4E)]^{1/3}F_{max}^{5/6}, \tag{34}$$

where F_{max} is given by Eq. (32).

The yield velocity at which plastic deformation must be taken into account can be calculated from Eq. (31) by using $F_{max} = F_1$. This velocity is

$$V_y = \sqrt{\frac{4}{5}\frac{F_1\delta_1}{m}}. \tag{35}$$

The yield velocity in terms of material properties and incident parameters is given by

$$V_y = \delta_1\sqrt{\frac{4}{5}\eta R/m} = \frac{9}{8\sqrt{5}}E^{-2}\eta^{5/2}R^{3/2}m^{-1/2}. \tag{36}$$

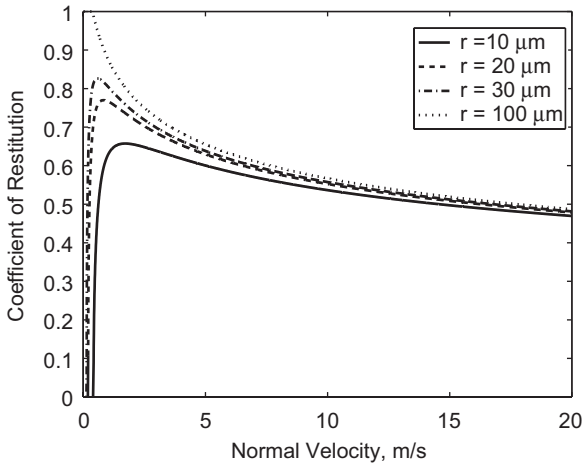

Fig. 2. The coefficient of restitution versus normal velocity for the impact of different-size aluminum-oxide microspheres with an aluminum surface.

An analytical solution for adhesive elastic–plastic impact can be obtained by assuming that the work dissipated due to plastic deformation and the work dissipated due to adhesion are additive. The final coefficient of restitution becomes

$$e = \sqrt{e_{\mathrm{pl}}^2 + e_{\mathrm{A}}^2 - 1}, \tag{37}$$

where $e_{\mathrm{A}} = \sqrt{1 - 2W_{\mathrm{A}}/(mv^2)}$ and e_{pl} is determined by Eq. (34).

An illustration of the EAP-model coefficient of restitution calculated for different radii (10, 20, 30, and 100 μm) of an aluminum oxide particle ($E = 360$ GPa and $\nu = 0.23$) impacting an aluminum surface ($E = 70$ GPa and $\nu = 0.35$) is presented in Fig. 2. The plastic constant for this case is $k = \sigma_{\mathrm{T}}/2 = 290$ MPa. The yield velocity equals 0.37 m/s. For all radii, starting at normal velocities greater than approximately 2 m/s, the coefficient of restitution monotonically decreases toward zero as the normal velocity is increased.

Below approximately 2 m/s, different trends occur. For the largest radius examined, the coefficient of restitution increases to a value of unity as the normal velocity is decreased. At a velocity of approximately 0.01 m/s, the capture velocity for this diameter microsphere, the microsphere is captured by the surface. This is indicated by a very rapid decrease in the coefficient of restitution, which occurs slightly above the critical velocity. Similar, less pronounced trends are seen for the smaller radii microspheres. Their values of the coefficient of restitution increase with decreasing normal velocity but never reach unity. This primarily is the result of adhesion forces, which are significant for small particles. In the model, if a particle impacts the surface at velocities greater than V_{y}, then plastic effects are taken into account. If velocity is less then V_{y}, then no plastic effects are considered. The definitional domain of the model is from the capture velocity up to velocities where all of the microsphere's incident kinetic energy is dissipated into the heat through plastic deformation. This velocity domain corresponds to the values of the coefficient of restitution from zero to unity.

5. Surface roughness effects

Surface roughness can significantly reduce adhesion. In order to compare theory with experiment, surface roughness must be included in an adhesion model (Ingham & Yan, 1994; Ziskind, Fichman, & Gutfinger, 1997). Cheng et al. (2002b) showed that increasing surface roughness reduces the pull-off force and decreases the tendency for a microsphere to snap-on and snap-off of the surface. The problem of describing of surface roughness is multi-dimensional because the surface has a wide range of scales in height and length. Following Cheng's work, the surface is assumed to have submicrometer and nano-scale roughnesses. Greenwood and Williamson (1966) showed that surface roughness heights have a Gaussian distribution about the mean surface. If the distance from the mean surface is s, then the probability

distribution function of s is

$$\phi(s) = \frac{1}{\sqrt{2\pi}\sigma_s} e^{-s^2/2\sigma_s^2}, \tag{38}$$

where σ_s^2 is the variance of the roughness heights.

The Johnson, Kendall, and Roberts (JKR) and Derjaguin, Muller, and Toporov (DMT) theories occur at the two limits of Tabor's parameter (Maugis, 1992). This parameter is

$$\mu_T = \left(\frac{\gamma_{12}^2 r}{E^2 \varepsilon^3}\right)^{1/3}, \tag{39}$$

which represents the ratio of elastic displacement of surface at the point of separation to the equilibrium spacing, ε. Tabor (1977) also considered the effect of surface roughness on surface forces and surface interaction. He showed that this effect can be described in terms of an adhesion parameter, which is defined as

$$\theta = \frac{E\sigma_s^{3/2} r^{1/2}}{r w_A}. \tag{40}$$

The numerator is proportional to the elastic forces required to push a sphere of radius, r, to a depth of, s, into an elastic solid of modulus, E. The denominator is a measure of an adhesive force acting on a sphere of radius r. The adhesion parameter represents the competitive effect between the compressive forces influenced by high asperities that separate the contacting surfaces and the adhesion forces of lower asperities that hold the surfaces together. The smaller the value of θ, the higher the adhesion force. The higher the surface roughness, the larger the adhesion parameter and, thus, the adhesion force acquires a lower value.

By using a self-consistent model, Cheng et al. (2002b) also showed that microparticle adhesion is determined not only by the value of Tabor's parameter but also by the roughness height. By using the coefficient $C_R = F_p/F_{po}$, the reduction of the adhesion force due to roughness can be accounted for. According to Cheng's work, this coefficient decreases from 1 to 0.05 as the standard deviation of the asperity heights increases from 0 to 5 Å. Beyond 5 Å, C_R continues to decrease monotonically towards 0. This model has been verified indirectly by Ibrahim, Dunn, and Brach (2003).

6. Experimental validation of the model

The results of experiments of several different investigators were used to validate the EA and EAP models. These include the normal-incidence impact experiments of Dahneke (1973, 1975), Wall et al. (1990), Dunn, Brach, and Caylor (1995), and Li, Dunn, and Brach (1999), and the oblique-incidence experiments of Dunn, Brach, and Janson (1996), and Li, Dunn, and Brach (2000). Also included are the experimental results of Gorham and Kharaz (2000) who carried out normal and oblique experiments showing plastic effects. The material properties and parameters used in this study and presented by different authors are shown in Tables 1 and 2.

6.1. EA validation experiments

6.1.1. Normal incidence

Wall et al. (1990) measured the incident and rebound velocities of ammonium fluorescein microspheres of different diameters (2.58, 3.44, 4.9, and 6.89 μm). The velocity range was from approximately 1–100 m/s with adhesion effects evident below about approximately 15 m/s.

Dahneke (1973, 1975) reported measurements of the bouncing of small latex spheres. He measured both the incident and rebound velocity of polystyrene latex spheres impacting polished quartz, gold/glass, polystyrene surfaces in a vacuum chamber, at pressures less than 10^{-4} Torr. The range of the incident velocity was from approximately 2.5–35 m/s.

Dunn et al. (1995) carried out experiments on both the normal and oblique impact of polydisperse microspheres (stainless steel, silver-coated glass, and nickel) with planar surfaces (stainless steel, aluminum, Tedlar, and copper). The incident angles were from 20° to 90°. The normal incident velocity ranged from 2 to 25 m/s, which was not low enough to observe capture of the microsphere by the surface. Using a single-component phase Doppler particle analyzer

Table 1
Material properties

Material	ϱ (kg/m^3)	ν	E (GPa)	$k \cdot 10^{-12}$	γ_{theory}[a] (J/m^2)	γ_{exp} (J/m^2)	σ_T (MPa)
Silicon	2330	0.28	166	1.8	1.42	1.14–1.23[b,c]	120
Mica	2600–3200	0.3	90	3.2	0.77	4.50	N/A
Molybdenum	10 280	0.31	329	8.8	2.81	–	300–415
Tedlar	1460	0.33	2.1	28.8	0.018	0.03[d]	N/A
Stainless steel	8000	0.27	190	1.6	1.62	0.70–1.10	310
Aluminum	2700	0.33	69	4.1	0.59	1.14, 1.16[b,c]	21
Polystyrene	1040–1070	0.33	3–3.5	81.0–94.6	0.025–0.030	0.04[c]	90
Copper	8940	0.34	130	2.2	1.11	1.79, 1.83[b,c]	33–333
Ag-coated glass	1350	0.33	1.2	4.2	0.61	–	N/A
Ammonium fluorescein	1350	0.33	1.2	236.4	0.01	–	N/A

[a]Gilman (1960).
[b]Tyson and Miller (1977).
[c]de Boer, Broom, Mattens, Miedema, and Niessen (1988).
[d]www.mcloone.com.

Table 2
The work of adhesion and Hertzian stiffness for various experiments

Surface material	Particle material	Work of adhesion (J/m^2)	Stiffness K (GPa)	Author
Silicon	Amm. fluorescein	0.24	1.8	Wall
Mica	Amm. fluorescein	0.18	1.8	Wall
Molybdenum	Amm. fluorescein	0.34	1.7	Wall
Tedlar	Amm. fluorescein	0.03	1.6	Wall
Stainless steel	Ag-coated glass	1.99	73.4	Caylor
Copper	Ag-coated glass	1.65	66.4	Caylor
Aluminum	Ag-coated glass	1.20	50.9	Caylor
Tedlar	Ag-coated glass	0.21	12.9	Caylor
Silicon	Stainless steel	3.03	127.8	Li
Polished quartz	Polystyrene	0.24	1.2	Dahneke

system, the incident and rebound normal velocities, particle size, and crossing time were obtained. From the known information on particle velocity before and after the impact, the coefficient of restitution was found.

Li et al. (1999) experimentally investigated the normal impact of polydisperse microspheres with surfaces. The incident and rebound velocity components and particle size were measured using the phase Doppler approach. Incident normal velocities were slightly higher than those required for particle capture by the surface.

The comparison between the experimental data and results given by the present model for the normal coefficient of restitution are shown in Figs. 3–6. The experimental data are shown by circles. Error bars are plotted for those cases where uncertainty analysis could be performed. Because no surface roughness data were given for the experiments except for Li's surfaces and Wall's molybdenum surface, the coefficient C_R was best fitted. Its value was in the range of 0.43–0.82, which corresponds to those typical of highly polished surfaces. The mean roughness height for Li's data for the silicon surface was 1 nm and the roughness height of the molybdenum surface in Wall's experiment was less than 5 nm. The solid curve on each plot depicts EA model predictions with the best-fitted coefficients C_A and C_H. The dashed curve illustrates EA model predictions when no energy dissipation is assumed (when C_A and C_H equal zero).

Fig. 3 shows the measured (Wall et al., 1990) and calculated coefficients of restitution versus the incident normal velocity for ammonium fluorescein particles of 2.58, 3.44, and 4.9 μm diameter impacting a silicon surface. The coefficients C_A and C_H were best-fitted for the smallest diameter and then used for larger diameters, because materials remained the same. Fig. 4 demonstrates the dependence of the coefficient of restitution on the normal incident velocity for ammonium fluorescein particles of 3.44 μm diameter impacting molybdenum and mica surfaces. The comparison of the EA model and Dahneke's data for polystyrene particles of 1.26 μm diameter impacting the quartz surface are presented in Fig. 5.

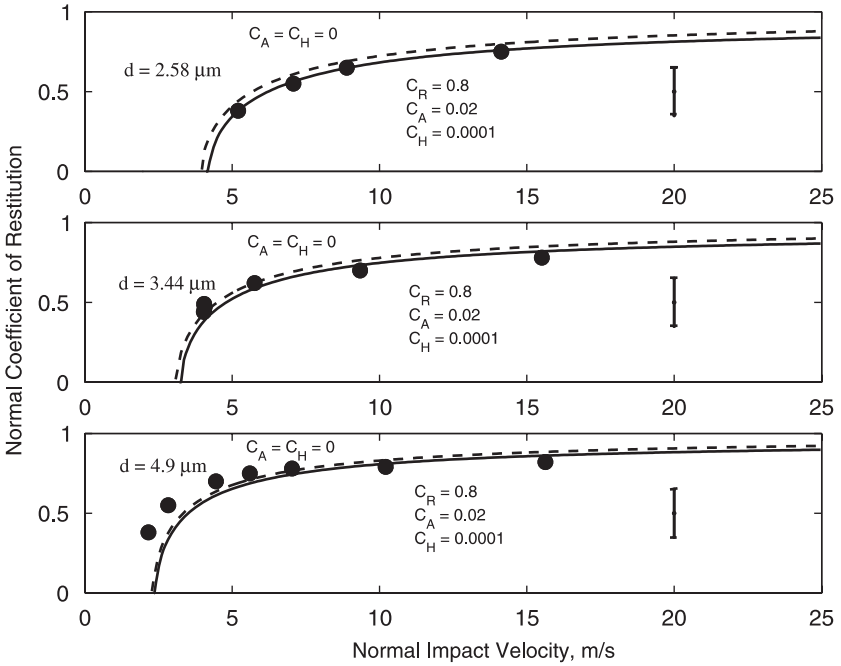

Fig. 3. Coefficient of restitution versus normal velocity. Data (circles) of Wall et al. (1990) for ammonium fluorescent microsphere impact with a silicon surface. EA model without dissipation (dashed curve); EA model with dissipation (solid curve).

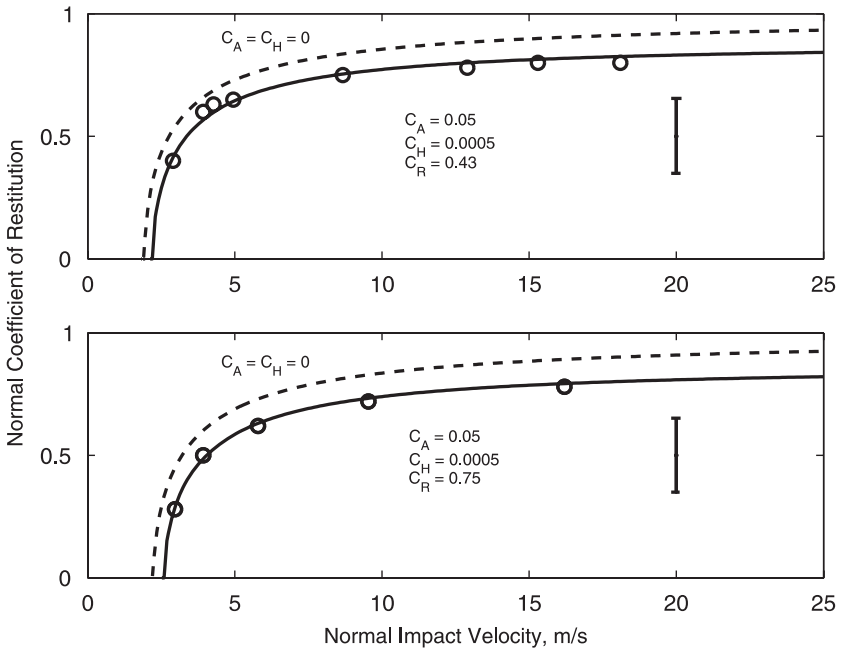

Fig. 4. Coefficient of restitution versus normal velocity. Data (circles) of Wall et al. (1990) for ammonium fluorescent microsphere impact with a molybdenum surface (top) and a mica surface (bottom). EA model without dissipation (dashed curve); EA model with dissipation (solid curve).

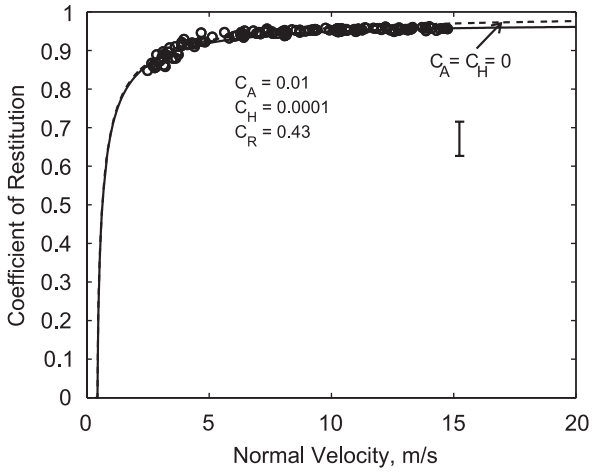

Fig. 5. Coefficient of restitution versus normal velocity. Data (circles) of Dahneke (1975) for 1.27 μm diameter latex microsphere impact with a quartz surface. EA model without dissipation (dashed curve); EA model with dissipation (solid curve).

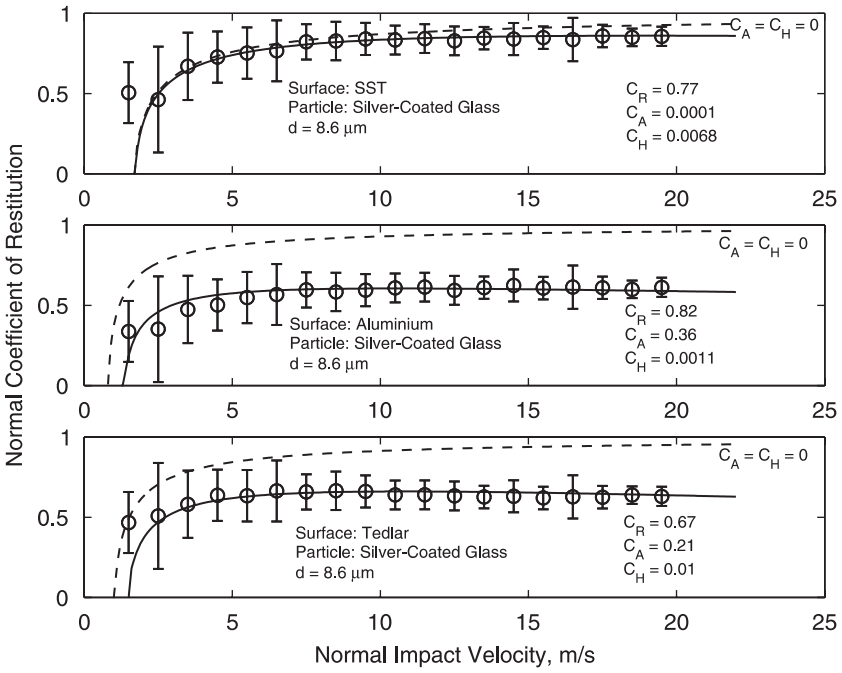

Fig. 6. Coefficient of restitution versus normal velocity. Data (circles) of Dunn et al. (1995) for Ag-coated glass microsphere impact with various surfaces. EA model without dissipation (dashed curve); EA model with dissipation (solid curve).

Fig. 6 displays the measured (Dunn et al., 1995) and the calculated normal coefficient of restitution versus the incident normal velocity for silver-coated glass microspheres impacting three different surfaces. The cases of aluminum and Tedlar surfaces show that damping properties of materials play essential role and must be taken into account. For all nine cases, the normal coefficient of restitution is relatively constant for high velocities and decreases with decreasing incident velocity. Below ∼5 m/s, the coefficient of restitution gradually approaches zero. Eventually particle capture occurs at a critical velocity. Further, the coefficient of restitution for the same initial normal velocity is greater for larger values of Young's modulus for the surface. More energy is dissipated through damping for softer surfaces.

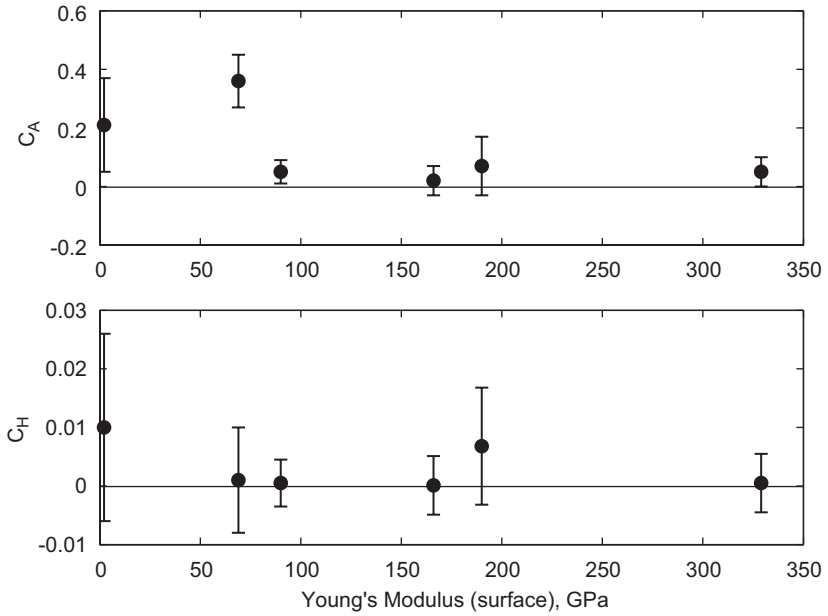

Fig. 7. Damping coefficients versus Young's modulus of the surface.

It follows from the model that for greater coefficients C_A and C_H, more energy is dissipated. Thus, there is a correlation between the softness of the material and damping coefficients C_A and C_H; the softer the material, the larger the values of the damping coefficients, as seen in Fig. 7. The best correlations between the C_A and C_H values were obtained with Young's modulus values of the surface. Weaker correlations were obtained with Young's modulus values of the particle or with those of the surface and particle combined.

For all cases presented in Figs. 3–6, the EA model with best-fitted C_A and C_H values agrees with the data to within the experimental uncertainty, which typically is approximately 20%. Further, the EA model with no dissipation forces agrees with the data to within the experimental uncertainty for all cases except the softer aluminum and Tedlar surface cases shown in Fig. 6.

6.1.2. Oblique incidence

Fig. 8 illustrates the measured and calculated normal coefficients of restitution and impact ratios for oblique impact. The data were obtained by Dunn et al. (1996) and Li et al. (2000) for SiO_2 surfaces and stainless steel particles with a mean diameter of 70 μm. In the model used for comparison, it is assumed that coefficient of friction is constant and that the initial angular velocity of particles, ω, is equal to zero. In the case of the normal impact (when $\alpha_i = 90°$), no tangential force will develop and, thus, $\mu = 0$. If $\omega \neq 0$, then the value of μ will be above or below the abscissa, depending upon the direction of rotation.

For all cases presented in Fig. 8, the EA model with best-fitted C_A and C_H values agrees with the data to within the experimental uncertainty, which typically is approximately 15%. Also, the EA model with no dissipation forces agrees with the impulse ratio data to within the experimental uncertainty, but not with the coefficient of restitution data to within that degree.

6.2. EAP validation experiments

Gorham and Kharaz (2000) conducted normal and oblique impact experiments to examine the variation of e with velocity for the combination of aluminum oxide particles ($E = 360$ GPa, $\nu = 0.23$) and aluminum anvil (E = 70 GPa, $\nu = 0.35$). The results of their experiments are shown in Fig. 9a as circles and squares. The plastic constant for these experiments equals 290 MPa. The uncertainty in these experiments was less than approximately 2% of the variable

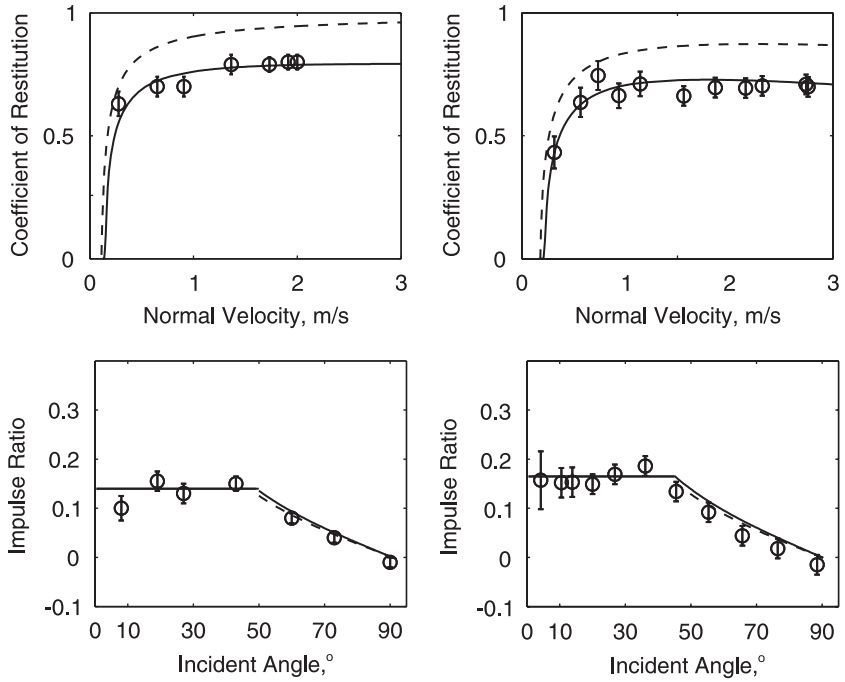

Fig. 8. Coefficient of restitution versus normal velocity (top) and impulse ratio versus incidence angle (bottom). Data (circles) of Dunn et al. (1996) (left column) and of Li et al. (2000) (right column) for 70 μm diameter (mean) stainless steel microsphere impact with a silicon surface. EA model without dissipation (dashed curve); EA model with dissipation (solid curve with $C_A = 1.3$ and $C_H = 0.007$). $C_R = 0.15$ for both model cases.

value. The coefficient of restitution decreased from over 0.83 at 0.45 m/s to less than 0.57 at 6.3 m/s as plastic effects increased.

The dashed curve in Fig. 9a represents the theory of Tabor (1948). In his theory, the rebound and incident velocities are linked through the equation

$$V = \kappa(v^2 - \beta V^2), \tag{41}$$

where κ is a constant depending on the materials and β is a function of work-hardening, which is related to Meyer's index, n, by

$$\beta = (2n - 1)/(2n + 4). \tag{42}$$

The constant κ is expressed in terms of β and the yield velocity, V_y, by

$$\kappa = \frac{V_y}{(V_y^2 - \beta V_y^2)^\beta}. \tag{43}$$

The best-fitted values for the yield velocity and Meyer's index are 0.09 m/s and 2.29, respectively.

The dashed-dotted curve corresponds to the theory of Thornton and Ning (1998). In his theory, the expression for the coefficient of restitution for elastic–perfectly plastic spheres is

$$e = \left(\frac{6\sqrt{3}}{5}\right)^{1/2}\left[1 - \frac{1}{6}\left(\frac{V_y}{v_n}\right)^{1/2}\right]\cdot\left[\frac{(V_y/v_n)}{(V_y/v_n) + 2\sqrt{\frac{6}{5} - 0.2(V_y/v_n)^2}}\right]^{1/4}. \tag{44}$$

The solid curve in Fig. 9a corresponds to Eq. (34). All curves in the figure decrease monotonically to lower values of the coefficient of restitution. Thornton's theory overestimates the data. The EAP model agrees with the data to within the experimental uncertainty.

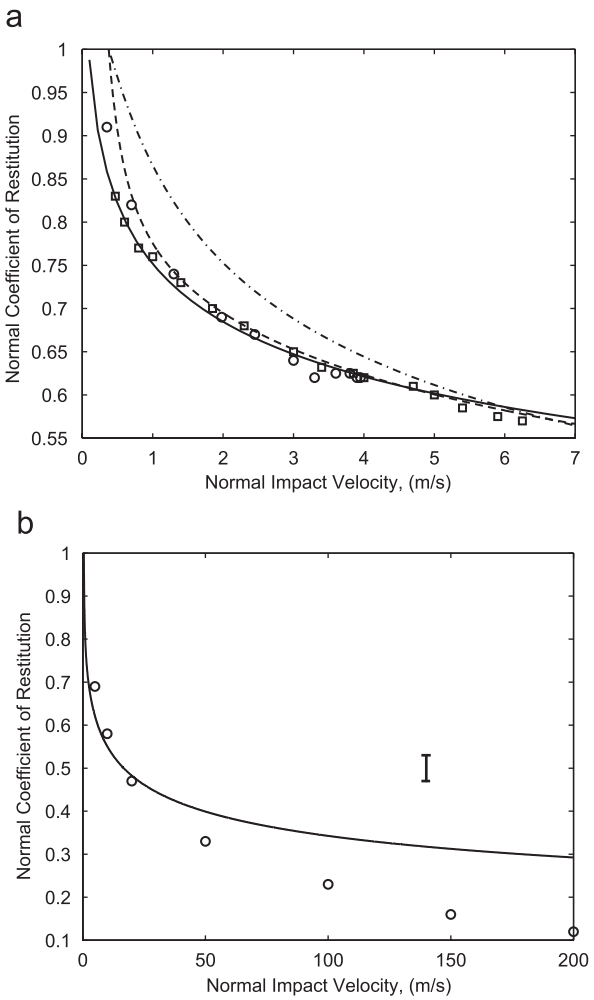

Fig. 9. Coefficient of restitution versus normal velocity. Aluminum surface, aluminum oxide particle with the diameter of 5 mm. Normal impact data (circles) and oblique impact data (squares). (a) Data of Gorham and Kharaz (2000) for 5 mm diameter aluminum-oxide sphere impact with an aluminum surface. EAP model (solid curve); Tabor's model (Eq. (41)) (dashed curve); Thornton and Ning's model (Eq. (44)) (dotted-dashed curve). (b) Data of Kangur and Kleis (1988) for 1.29 mm-diameter stainless steel sphere impact with a stainless steel surface. EAP model (solid curve).

The EAP model is compared with the higher-velocity data of Kangur and Kleis (1988) in Fig. 9b. In their experiments, stainless steel particles impacted a massive stainless-steel plate. The plastic constant for this case equals 480 MPa. The EAP model agrees with the data to within the experimental uncertainty except at velocities greater than approximately 25 m/s. At such large velocities, the model assumption that the particle's contact radius is small compared to its normal radius becomes invalid.

7. New validation experiment

A schematic of the experimental apparatus used for the new validation experiment is shown in Fig. 10 (see Ibrahim et al., 2003, for further detail). Air is drawn through this in-draft wind tunnel through the test section used to study microparticle transport and impact behavior. For this experiment, the mean flow velocity was 2 m/s, and the air temperature and relative humidity were 24 °C ± 2 °C and at 25%, respectively.

Hundred μm diameter copper microspheres were dispersed into the main flow using a mechanical microparticle dispenser located at the upper surface of the wind tunnel. The dispersed microspheres were transported by the flow along the tunnel and fell onto a glass substrate embedded in the bottom surface of the wind tunnel at a distance

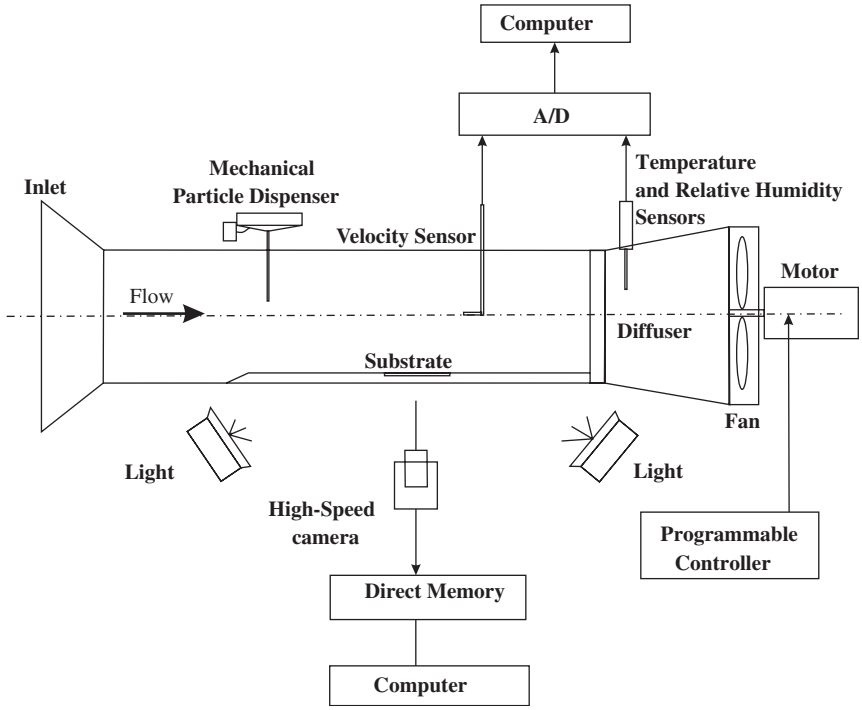

Fig. 10. Schematic of the wind tunnel used for new validation experiments.

of 7 cm downstream from the particle dispenser. A digital high-speed camera (Fastcam ultraAPX IMAGER, Fotron, ThorLABSinc) was used to track particles at 4000 frames/s. The data were analyzed using image processing software. These direct measurements gave incident and rebound angles, velocities, and trajectories of the impacting microspheres.

An algebraic approximation of the impact model was configured as a user-defined function (UDF) written in C++ language so that it could be implemented readily within the CFD software package FLUENT®. FLUENT® was used to compute the in-flight particle trajectories before and after particle contact with a surface, and either the model's UDF or a FLUENT®-specified boundary condition was used for the contact phase.

FLUENT® models particle impact with a surface through one of four possible specified boundary conditions: (1) *trap*, which terminates the trajectory calculations and records the fate of the particle as trapped by the surface, (2) *escape*, which considers the particle as having escaped back into the flow after it encounters the surface, (3) *wall-jet*, which determines the direction and particle velocity of a rebounding particle through momentum flux as a function of the impingement angle, and (4) *reflect*, which uses specified normal and tangential coefficients of restitution.

For the *reflect* boundary condition, the coefficients, e and μ, each are expressed in terms of the incident angle, α_i, and empirical coefficients one of the three expressions of ϕ for either e or μ:

- polynomial: $\phi = A_1 + A_2\alpha_i + A_3\alpha_i^2 + \cdots$
- piecewise-linear: $\phi = \phi_n + (\phi_{n+1} - \phi_n)\ (\alpha - \alpha_{in})/(\alpha_{in+1} - \alpha_{in})$, where $1 \leqslant n \leqslant N$, and N is the number of segments, and
- $\phi = A_1 + A_2\alpha_i + A_3\alpha_i^2 + \cdots$ when $\alpha_{i\,\min 1} \leqslant \alpha_i \leqslant \alpha_{i\,\max 1}$ or $\phi = B_1 + B_2\alpha_i + B_3\alpha_i^2 + \cdots$ when $\alpha_{i\,\min 2} \leqslant \alpha_i \leqslant \alpha_{i\,\max 2}$.

For particles with diameters less than approximately 100 μm, it is necessary to use a surface-contact model that considers adhesion. An explicit expression for the coefficient of restitution, such as that given by Eq. (24) can be incorporated in FLUENT® via a UDF for boundary conditions of the discrete (particle) phase.

A comparison between a FLUENT® simulation using an EA model UDF with no dissipation forces and data is presented in Fig. 11a, in which the trajectory of copper microsphere impacting a glass surface is shown. Air flow is from left to right. Before the microsphere is captured by the surface, it bounces off of the surface two times.

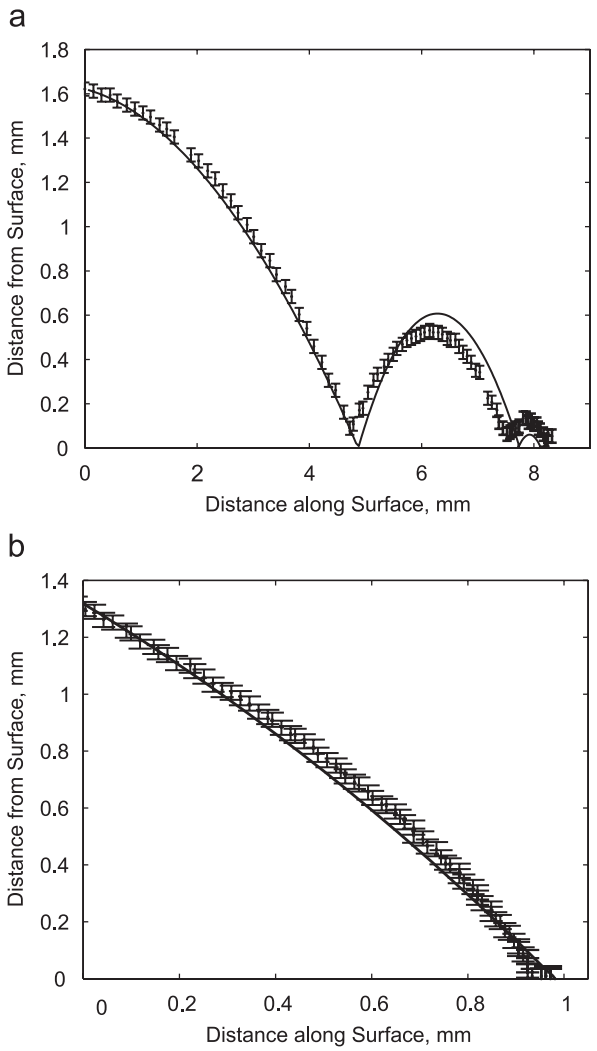

Fig. 11. Microsphere trajectories in the vertical plane. Data (points with error bars) and FLUENT® simulation with EA model UDF without dissipation and $C_R = 0.8$ (solid curve); (a) 90 μm diameter copper microsphere impact with a glass surface; (b) 61 μm diameter copper microsphere impact with a glass surface.

With each bounce, some of the microsphere's kinetic energy is dissipated. The data are indicated by circles with error bars and the simulation results are shown by the solid line. The simulation agrees with the data to within the experimental uncertainty up to the first impact. There is noticeable disagreement after each rebound because within FLUENT®, the instance of surface contact is considered to be when the particle's center of mass reaches the wall. In fact, contact forces begin to act just before the particle reaches the surface, and actual contact is made on radius *before* the center of mass would theoretically reach the wall. Another instance of capture is shown in Fig. 11b. Here, the particle velocity is small enough for the particle to be captured by the surface. Almost all of its incident kinetic energy is transformed into adhesion work.

A comparison between two simulations is shown in Fig. 12. Both simulations were made for the transport and impact of a 70 μm diameter Ag-coated glass microsphere onto an aluminum surface. In one simulation the EA model-based UDF is used, in the other FLUENT®'s *reflect* condition with for the idealized case of $e = 1$. The microsphere's initial position is shown by point A. Its initial velocity is 3.5 m/s in the upward vertical direction. Air flow is from left to right and its mean velocity is 2 m/s. The microsphere rebounds from the top wall and eventually is captured by the lower-wall surface. For the idealized case of totally elastic impact, the distance along the surface until capture is

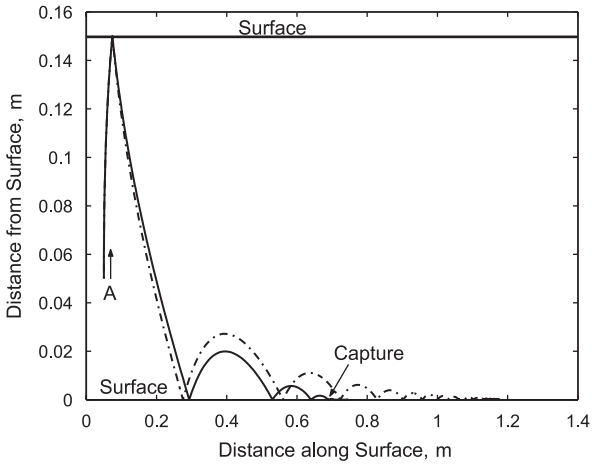

Fig. 12. Simulations of trajectories of a 70 μm diameter Ag-coated glass microsphere impact with an aluminum surface. FLUENT® simulation with EA model UDF (solid curve) and with *reflect* boundary condition with $e = 1$ (dotted-dashed curve).

approximately twice that of the case utilizing the EA model-based UDF. It should be noted that even in the idealized case, the microsphere's kinetic energy is dissipated through aerodynamic drag while in the air flow.

8. Conclusions

Empirically validated models of particle-surface impact were presented that can be used in multi-phase CFD simulations. Specifically, two models based upon analytical solutions of the governing equations of microsphere impact with a surface were presented. The EA model considered elastic impact with adhesion and included the effects of elastic and adhesion dissipation. The EAP model additionally considered plastic effects that could arise with ductile materials. Both models were validated by comparison with the data of a number of investigators. Model validation was achieved to within experimental uncertainty, which typically was 15% or less, for all cases considered below approximately 25 m/s. Explicit expressions derived from the model were developed as a UDF that could be incorporated into a CFD software package that considers a discrete particle phase. Additional validation experiments were conducted in a wind tunnel using high-speed digital microphotography for simulation comparison purposes. FLUENT® simulations using either the developed UDF or FLUENT®'s specified boundary condition were compared with observed particle motion.

Acknowledgments

Research described in this article was supported by Philip Morris USA Inc. and Philip Morris International.

References

Alexandrov, V. M., Kadomtsev, I. G., & Tsaryuk, L. B. (1984). Axisymmetric contact problems for elastoplastic bodies. *Trenie Iznos*, *1*, 16–26.

Andres, R. P. (1995). Inelastic energy transfer in particle/surface collision. *Aerosol Science and Technology*, *23*, 40–50.

de Boer, F. R., Broom, R., Mattens, W. C. M., Miedema, A. R., & Niessen, A. K. (1988). *Cohesion in Metals*. Amsterdam: Elsevier.

Brach, R. M., & Dunn, P. F. (1995). Macrodynamics of microparticles. *Aerosol Science and Technology*, *23*, 51–71.

Brach, R. M., Dunn, P. F., & Li, X. (2000). Experiments and engineering models of microparticle impact and deposition. *Journal of Adhesion*, *74*, 227–282.

Biryukov, D. G., & Kadomtsev, I. G. (2002). Dynamic elastoplastic interaction between an impactor and a spherical shell. *Journal of Applied Mechanics and Technical Physics*, *43*, 777–781.

Cheng, W., Brach, R. M., & Dunn, P. F. (2002a). Three-dimensional modeling of microsphere contact/impact with a smooth, flat surface. *Aerosol Science and Technology*, *36*, 1045–1060.

Cheng, W., Brach, R. M., & Dunn, P. F. (2002b). Surface roughness effects on microparticle adhesion. *Journal of Adhesion*, *78*, 929–965.

Dahneke, B. (1973). Measurements of the bouncing of small latex spheres. *Journal of Colloid and Interface Science*, *45*, 584–590.

Dahneke, B. (1975). Further measurements of the bouncing of small latex spheres. *Journal of Colloid and Interface Science*, *51*, 58–65.

Dunn, P. F., Brach, R. M., & Caylor, M. J. (1995). Experiments on the low-velocity impact of microspheres with planar surfaces. *Aerosol Science and Technology*, *23*, 80–95.

Dunn, P. F., Brach, R. M., & Janson, G. G. (1996). Surface contact mechanics during oblique impact of microspheres with planar surfaces. *Aerosol Science and Technology*, *25*, 445–465.

Gilman, J. (1960). Direct measurements of the surface energies of crystals. *Journal of Applied Physics*, *31*(12), 2208–2217.

Gorham, D. A., & Kharaz, A. H. (2000). The measurements of particle rebound characteristics. *Powder Technology*, *112*, 193–202.

Greenwood, J. A., & Williamson, J. B. P. (1966). Contact of nominally flat surfaces. *Proceedings of the Royal Society of London. Series A*, *295*, 300–319.

Hunter, S. C. J. (1957). Energy absorbed by elastic waves during impact. *Journal of Mechanics and Physics of Solids*, *5*, 162–171.

Ibrahim, A., Dunn, P. F., & Brach, R. M. (2003). Microparticle detachment from surfaces exposed to turbulent air flow: Controlled experiments and modeling. *Journal of Aerosol Science*, *34*, 765–782.

Ingham, D. B., & Yan, B. (1994). Re-entrainment of particles on the outerwall of a cylindrical blunt sampler. *Journal of Aerosol Science*, *25*, 327–340.

Israelachvilli, J. N. (1992). *Intermolecular and surface forces*. (2nd ed.), San Diego: Academic Press.

Kangur, H. F., & Kleis, I. R. (1988). Experimental and theoretical determination of the coefficient of restitution. *Izvestie AN USSR. MTT.*, *5*, 182–185 (in Russian).

Klinkov, S. V., Kosarev, V. F., & Rein, M. (2005). Cold spray deposition: significance of particle impact phenomena. *Aerospace Science and Technology*, *9*, 582–591.

Li, X., Dunn, P. F., & Brach, R. M. (1999). Experimental and numerical studies on microsphere normal impact with surfaces. *Journal of Aerosol Science*, *30*, 439–449.

Li, X., Dunn, P. F., & Brach, R. M. (2000). Experimental and numerical studies of microsphere oblique impact with planar surfaces. *Journal of Aerosol Science*, *31*, 583–594.

Maugis, D. (1992). Adhesion of spheres: The JKR-DMT transition using a Dugdale model. *Journal of Colloid and Interface Science*, *150*, 243–269.

Sagomonyan, A. Y. (1988). *Dynamics of obstacle destruction*. Moscow: Moscow State University, (in Russian).

Tabor, D. (1948). A simple theory of static and dynamic hardness. *Proceedings of the Royal Society of London. Series A*, *192*, 247–274.

Tabor, D. (1977). Surface forces and surface interactions. *Journal of Colloid and Interface Science*, *58*, 2–13.

Thornton, C., & Ning, Z. (1998). A theoretical model for the stick/bounce behavior of adhesive, elastic–plastic spheres. *Powder Technology*, *99*, 154–162.

Timoshenko, S., & Goodier, J. N. (1951). *Theory of elasticity*. (2nd ed.), New York: McGraw-Hill.

Tsai, C. J., Pui, D. Y. H., & Liu, B. Y. H. (1991). Capture and rebound of small particles upon impact with solid surfaces. *Aerosol Science and Technology*, *12*, 497–507.

Tyson, W. R., & Miller, W. A. (1977). *Surface Science*, *62*, 267and references therein.

Wall, S., John, W., Wang, H. C., & Goren, S. L. (1990). Measurements of kinetic energy loss for particles impacting surfaces. *Aerosol Science and Technology*, *12*, 926–946.

Xu, M., & Willeke, K. (1993). Right-angle impaction and rebound of particles. *Journal of Aerosol Science*, *24*, 19–30.

Ziskind, G., Fichman, M., & Gutfinger, C. (1997). Adhesion moment model for estimating particle detachment from a surface. *Journal of Aerosol Science*, *28*, 623–634.